

Primordial black holes versus their impersonators at gravitational wave observatories

Andrea Begnoni^{a,b} and Stefano Profumo^{c,d}

^aDipartimento di Fisica Galileo Galilei, Università di Padova, I-35131 Padova, Italy

^bINFN Sezione di Padova, I-35131 Padova, Italy

^cSanta Cruz Institute for Particle Physics,
Santa Cruz, CA, 95064, USA

^dDepartment of Physics, University of California, Santa Cruz
Santa Cruz, CA, 95064, USA

E-mail: andrea.begnoni@phd.unipd.it, profumo@ucsc.edu

Abstract. The detection of primordial black holes (PBHs) would mark a major breakthrough, with far-reaching implications for early universe cosmology, fundamental physics, and the nature of dark matter. Gravitational wave observations have recently emerged as a powerful tool to test the existence and properties of PBHs, as these objects leave distinctive imprints on the gravitational waveform. Notably, there are no known astrophysical processes that can form sub-solar mass black holes, making their discovery a compelling signal of new physics. In addition to PBHs, we consider other exotic compact object (ECO) candidates—such as strange quark stars and boson stars—which can produce similar gravitational signatures and potentially mimic PBHs. In this work, we employ the Fisher matrix formalism to explore a broad parameter space, including binary masses, spins, and a variety of nuclear and quark matter equations of state. Our goal is to assess the ability of next-generation gravitational wave detectors—specifically Cosmic Explorer and the Einstein Telescope—to distinguish PBHs from ECOs, stellar BHs and neutron stars. We compute the maximum luminosity distances at which confident ($\geq 3\sigma$) detections of sub-solar masses or tidal effects are possible, providing quantitative benchmarks for PBH identification or exclusion under various observational scenarios. Our results indicate that next-generation detectors will be capable of probing sub-solar mass PBHs out to cosmological distances of $z \sim 3$. For heavier objects with masses up to $M \lesssim 2M_\odot$, we show that PBHs can be distinguished from neutron stars via their lack of tidal effects up to redshifts of $z \sim 0.2$.

Contents

1	Introduction	1
2	Maximum luminosity distance	3
3	Theoretical and Observational Constraints on Strange Quark Stars	4
3.1	Equation of State Models and Mass Range	4
3.2	Lower Mass Limits and Ultra-Compact Stars	5
3.3	Pulsars and Gravitational Wave Observations on Tidal Deformability and Compactness	5
3.4	Spin Constraints and Angular Momentum	6
4	Theoretical and Observational Constraints on Boson Stars	7
4.1	Fundamental Properties and Mass Scaling	7
4.2	Rotating Boson Stars: Angular Momentum Quantization and Structure	8
4.3	Deviations from Black Hole Geometries	8
4.4	Astrophysical and Cosmological Implications	8
5	Lower Mass Limits of Neutron Stars	8
6	Primordial Black Holes	9
7	Methods and Assumptions	10
8	Results	11
9	Discussion and Conclusions	17
A	Technical details	18
A.1	Detectors	18
A.2	Tidal deformabilities	18

1 Introduction

The observation of gravitational waves (GWs) from compact binary mergers has opened a new avenue for probing fundamental physics, especially in the strong-field regime of general relativity [1–3]. Among the various imprints on GW signals, the effect of *tidal deformability*, characterized by Love numbers such as k_2 , plays an essential role in determining the internal structure and composition of compact objects during the late inspiral phase. The tidal deformability, quantified by the dimensionless parameter $\Lambda = (2/3)k_2(R/M)^5$, depends on the second Love number k_2 , the compactness $C = M/R$, and the mass-radius relationship of the merging objects [4, 5]. This makes tidal measurements a crucial diagnostic for distinguishing between primordial black holes (PBHs), light neutron stars (NSs), and exotic compact objects such as strange quark stars (SQSs) [6, 7].

A particularly interesting category of compact objects lies in the *sub-TOV mass regime*, where the object masses are below the maximum mass supported by the Tolman-Oppenheimer-Volkoff limit. In this mass range, the compactness C is lower than that of heavier neutron stars, resulting in significantly larger tidal deformability Λ for objects with material composition such as neutron stars or quark stars [4, 6]. In contrast, PBHs, which are pure vacuum solutions of Einstein’s field equations, possess zero tidal deformability ($k_2 = 0$) under classical general relativity [5–7]. This characteristic makes tidal effects, or their absence, a critical probe for identifying PBHs in gravitational wave observations of low-mass systems [6].

Tidal deformability encodes key properties of a compact object’s internal structure. For neutron stars, it depends strongly on the nuclear equation of state (EOS), which describes the relationship between pressure and density in dense matter [4, 8, 9]. At sub-TOV masses, where observational constraints on the EOS remain weak, the tidal imprint on the GW signal can provide a particularly sensitive probe. A stiffer EOS typically yields larger radii, which in turn leads to higher tidal deformability. In contrast, softer EOS models lead to more compact stars with reduced tidal signatures [6, 8]. For strange quark stars, which are governed by the EOS of self-bound quark matter, tidal deformability is suppressed compared to neutron stars of the same mass. However, their distinct tidal profiles, especially under EOS models such as the MIT bag model or color-flavor-locked quark phases, could still make them discernible in GW signals [4, 8, 9].

Primordial black holes (PBHs), on the other hand, provide a null hypothesis in the search for tidal deformability effects. As non-material objects, PBHs have $k_2 = 0$, and thus leave no detectable tidal imprint in gravitational waveforms during the inspiral [5, 7]. This property distinguishes PBHs from both neutron stars and exotic compact objects. Furthermore, recent work has explored the possibility of environmental effects (e.g., transient perturbations due to surrounding matter or accretion) inducing small but nonzero tidal signatures in PBHs [7]. Although these effects may complicate their identification in some scenarios, any detection of $k_2 \neq 0$ for merging compact objects at subsolar masses would strongly disfavor the PBH hypothesis [6].

From a waveform modeling perspective, tidal effects enter the GW phase evolution at the 5th post-Newtonian (PN) order, significantly impacting the late inspiral phase of compact binary mergers. These effects are particularly prominent for sub-TOV mass objects, whose reduced compactness amplifies their tidal deformability, making the tidal effects more observable [4, 6, 10]. Accurate modeling of these high-PN corrections, incorporating EOS-specific predictions for k_2 and Λ , is essential for parameter estimation. Improper modeling of tidal effects could lead to errors in recovering intrinsic properties of the merger, such as component masses, radii, and the nature of the compact objects [4, 6, 10].

Upcoming GW observations from LIGO-Virgo O4/O5 and third-generation detectors such as Cosmic Explorer and Einstein Telescope are expected to offer substantially improved sensitivity to tidal deformability parameters [6, 8, 11]. Precise measurements of Λ could allow for the confident classification of sub-TOV mass compact objects, distinguishing material systems (e.g., neutron stars or quark stars) with large k_2 from PBHs with $k_2 = 0$. This would enable rigorous tests of exotic physics, such as the existence of strange quark stars and the role of primordial black holes in the early Universe [6, 9]. Moreover, subsolar mass compact objects present a unique opportunity to probe the nuclear EOS in a low-density regime where existing observational constraints remain scarce [4, 8, 9, 12].

Beyond these general considerations, a number of recent studies provide a deeper theoretical and observational context. Early work on binary tidal dynamics [13] and Bayesian

parameter estimation [14–18] established key methodologies for distinguishing exotic compact objects from neutron stars and black holes.

For strange quark stars, theoretical studies refined their maximum mass range [19] and assessed their observational signatures [20]. The Love number formalism has been sharpened by critical re-analyses [21], while exotic models such as gravastars have been shown to follow distinct I-Love-Q relations that nevertheless asymptotically approach the black hole limit [22]. At the same time, waveform modeling studies have highlighted significant systematics in tidal inference for neutron star mergers [23]. Moreover, incorporating EOS knowledge [24, 25] and model-independent extractions of neutron star tidal deformability have also been pursued, providing robust EOS constraints free of waveform systematics [26]. Furthermore, the first numerical-relativity simulations of subsolar-mass black holes merging with neutron stars reveal gaps in current waveform models [27].

Different signatures were developed to distinguish PBH from ECO, e.g., combining spin, eccentricity, and tidal deformability [28], or peculiar imprints based on gravitational-wave memory effects sourced by PBHs [29]. Dedicated searches for subsolar-mass neutron stars were also carried out [30], and astrophysical evidence for stiff EOS models [31] strengthens the multi-messenger approach to the issue.

In this work, we employ the recently released `GWJulia` code [32], which utilizes the Fisher matrix formalism—also known as the Fisher information matrix (FIM)—to simulate the detection of compact objects using third-generation (3G) gravitational wave detectors. The FIM has been widely applied in GW data analysis [33–36], including in studies focused on 3G detectors [37–44], and has proven to be a valuable tool for estimating uncertainties in future observations. In the high signal-to-noise ratio (SNR) limit, the FIM can provide meaningful insights into the results of full Bayesian parameter estimation; for a review of its limitations, see [33].

In the remainder of this study, we investigate the detectability of both sub-solar mass events and tidal deformability effects—key signatures that could rule out the primordial black hole hypothesis in the GW signal. We leverage the computational efficiency of the FIM approach to explore the parameter space of compact binary mergers, considering variations in mass ratio, total mass, spin configurations, and EOS-dependent tidal deformability. Our goal is to assess the potential of current and future GW observatories to distinguish between different types of compact objects and to constrain the nuclear EOS, particularly in the low-density regime. This analysis serves as a foundation for more detailed Bayesian studies of the sub-solar mass regime and unconventional EOS scenarios in the Universe.

2 Maximum luminosity distance

The Fisher matrix Γ_{ij} is defined as [35, 36]

$$\Gamma_{ij} \equiv - \left\langle \frac{\partial^2 \log \mathcal{L}(d|\boldsymbol{\theta})}{\partial \theta^i \partial \theta^j} \right\rangle_n, \quad (2.1)$$

where $\log \mathcal{L}(d|\boldsymbol{\theta})$ is the log-likelihood of the event of datastream d given the parameters $\boldsymbol{\theta}$ and the brackets $\langle \dots \rangle_n$ represent the ensemble average of the noise realization. The indices i and j run over all the parameters of the binary $\boldsymbol{\theta}$, which are

$$\mathcal{M}_c, q, \chi_1, \chi_2, d_L, \theta, \phi, \iota, \psi, t_{\text{coal}}, \Phi_{\text{coal}}, \Lambda_1, \Lambda_2$$

where \mathcal{M}_c is the chirp mass, $q = m_1/m_2$ is the mass ratio, $\chi_{1,2}$ is the longitudinal spin of the two objects, d_L is the luminosity distance, (θ, ϕ) represent the sky position, ι is the inclination angle, ψ is the polarization angle and t_{coal} , Φ_{coal} represent respectively the time and phase to coalescence. Finally, if the objects are NS or ECO, the tidal deformability is represented by $\Lambda_{1,2}$. The FIM is expected to provide a good approximation to full Bayesian analysis under certain conditions: sufficiently high signal-to-noise ratios (SNR), non-pathological regions of parameter space (i.e., where the waveform derivatives with respect to parameters are well-defined), and when estimating population-averaged parameters. The validity of the high-SNR approximation has been studied in the literature [33, 34, 38].

Our analysis focuses on the average properties of a large population of compact objects. In such scenarios, the Fisher matrix is expected to yield a good approximation to the median or mean precision of parameter estimates derived from full Bayesian inference. Specifically, we estimate the median luminosity distance at which a sub-solar mass compact object can be measured with a 3σ significance, using a simulated catalog of compact binary mergers. In particular, we look for the luminosity distance $d_{L,3\sigma}$ such that

$$m_{\text{PBH}} + 3\sigma(d_{L,3\sigma}) < 1M_{\odot}. \quad (2.2)$$

We explore a range of intrinsic parameters, including the component masses, spin configurations, and mass-dependent tidal deformabilities across different equations of state (EOS). The remaining extrinsic parameters—sky position, inclination angle, polarization angle, coalescence time, and coalescence phase—are sampled from the prior distribution of the compact object population. This allows us to focus on estimating the median maximum luminosity distance for achieving a 3σ detection of a sub-solar mass compact object. To facilitate a better understanding, we convert luminosity distances into redshifts using flat Λ CDM Planck cosmology [45].

3 Theoretical and Observational Constraints on Strange Quark Stars

3.1 Equation of State Models and Mass Range

Strange quark stars (SQSs) are hypothesized compact stars composed of deconfined up, down, and strange quarks. Their possible existence is rooted in the Bodmer–Witten hypothesis [46, 47], which proposes that strange quark matter (SQM) could be the true ground state of hadronic matter. The stability and properties of SQSs are governed by the equation of state (EOS) for SQM, which is sensitive to several microphysical parameters.

The most widely used EOSs for modeling SQSs include:

- **MIT Bag Model:** Describes SQM as a Fermi gas confined by a vacuum pressure (bag constant B). Typical values of $B^{1/4}$ range from 130 to 170 MeV, with lower B values allowing for more compact and massive stars [48].
- **Color-Flavor Locked (CFL) Phase:** Introduces a pairing gap Δ due to color superconductivity, which stiffens the EOS and raises both the maximum mass and the minimum mass for stability [49, 50].
- **Chromodielectric and Density-Dependent Mass Models:** These incorporate QCD-inspired confinement and medium effects, modifying the effective quark mass and coupling, thereby influencing the star’s compactness [51, 52].

- **Nambu–Jona-Lasinio (NJL) Model:** Includes interactions such as scalar and vector meson exchange. While it typically predicts softer EOSs, vector repulsion terms can yield stars with maximum masses up to $2.2\text{--}2.4 M_\odot$ [53, 54].

High-mass constraints from observations of pulsars such as PSR J0740+6620 ($M = 2.08 \pm 0.07 M_\odot$) [55] exclude overly soft EOSs. Meanwhile, stiffer versions of the MIT or CFL models remain viable.

3.2 Lower Mass Limits and Ultra-Compact Stars

Unlike neutron stars, whose lower mass limit is set by nuclear saturation and degeneracy pressure, SQSs could theoretically exist with significantly smaller masses. The stability of low-mass SQSs depends on whether strange quark matter is absolutely stable at zero pressure.

- **MIT Bag Model:** For low bag constants ($B^{1/4} \sim 145 \text{ MeV}$), studies suggest stable SQSs can exist with gravitational masses as low as $\sim 0.01 M_\odot$ [52]. Such objects would be exotic analogs to planets or brown dwarfs in mass, yet with much smaller radii ($\sim 2\text{--}4 \text{ km}$).
- **Chromodielectric Model:** Introduces medium effects in confinement, yielding stable SQS configurations down to $\sim 0.9 M_\odot$ with radii of $\sim 6 \text{ km}$ [51]. These stars are significantly more compact than neutron stars of comparable mass.
- **CFL Superconductivity and Surface Tension:** The presence of a CFL phase lowers the minimum stable mass by altering the balance between pressure and energy density [56]. Surface tension effects, which control the phase interface between hadronic and quark matter, further influence stability thresholds.

These models predict that SQSs may occupy parts of the mass-radius parameter space inaccessible to neutron stars, suggesting a class of compact stars that could be probed through high-resolution X-ray and gravitational wave observations.

3.3 Pulsars and Gravitational Wave Observations on Tidal Deformability and Compactness

Observational data from massive pulsars and gravitational wave detections place strong constraints on the viable parameter space for strange quark star (SQS) models. The discovery of PSR J0740+6620, with a mass of $2.08 \pm 0.07 M_\odot$ [55], sets a robust lower bound on the maximum mass that any realistic equation of state (EOS) must support. This effectively rules out overly soft quark matter EOSs, particularly those with high Bag constants B or weak quark interactions that cannot stabilize stars in this mass range. Stiff EOSs—achieved through lower B , inclusion of perturbative QCD corrections, or color-flavor-locked (CFL) superconductivity—remain viable and can produce stable SQSs with maximum masses above $2.1 M_\odot$.

Gravitational wave observations from binary compact object mergers provide complementary constraints, particularly on tidal deformability. The relevant parameter is the dimensionless tidal deformability Λ , which characterizes how easily a star is deformed by a companion’s tidal field and depends sensitively on the star’s compactness and internal structure. For an individual star, Λ is defined by

$$\Lambda = \frac{2}{3}k_2 \left(\frac{c^2 R}{GM} \right)^5, \quad (3.1)$$

where k_2 is the quadrupolar (second-order) Love number, R is the stellar radius, and M its gravitational mass.

In binary mergers, gravitational wave detectors are sensitive primarily to a mass-weighted combination of the two stars' tidal deformabilities, known as the combined tidal deformability $\tilde{\Lambda}$:

$$\tilde{\Lambda} = \frac{16}{13} \frac{(M_1 + 12M_2)M_1^4\Lambda_1 + (M_2 + 12M_1)M_2^4\Lambda_2}{(M_1 + M_2)^5}, \quad (3.2)$$

where M_1 and M_2 are the masses, and Λ_1 , Λ_2 are the tidal deformabilities of the two compact objects.

A commonly quoted reference value is $\Lambda_{1.4}$, the tidal deformability of a canonical 1.4, M_\odot compact star, which serves as a benchmark for comparing EOS models. Observations from GW170817 and subsequent analyses constrain $\tilde{\Lambda}$ to be $\lesssim 800$, with preferred ranges typically between 400 and 600 [57, 58]. Because strange quark stars tend to be more compact than neutron stars of the same mass, they generally have lower $\Lambda_{1.4}$ values. MIT Bag model-based SQS EOSs predict $\Lambda_{1.4}$ in the range ~ 300 –650, depending on the Bag constant B , perturbative QCD parameter a_4 , and the color-flavor-locked superconducting gap Δ [8, 9, 59]. Lower values of B yield more compact stars with smaller $\Lambda_{1.4}$, which in some cases may be too low and thus inconsistent with observational limits.

In summary, current pulsar mass measurements and gravitational wave constraints on tidal deformability place strong restrictions on strange quark star models, but a broad parameter space remains open. Models with moderate Bag constants and CFL phases can simultaneously satisfy maximum mass and tidal deformability bounds, leaving the astrophysical existence of strange quark stars a viable possibility.

SQSs, being more compact for a given mass, generally have smaller $\tilde{\Lambda}$ values than neutron stars.

- **Bag Constant Dependence:** Lower B leads to more compact stars with $\tilde{\Lambda}_{1.4} \lesssim 100$, while higher B produces less compact configurations with $\tilde{\Lambda}_{1.4} \approx 400$ –600, consistent with GW170817 constraints [8, 59].
- **Color Superconductivity:** The CFL phase slightly reduces $\tilde{\Lambda}$ by modifying the pressure-density relationship [60].
- **Model Sensitivity:** Quark mass, pairing gap, and perturbative QCD corrections all affect $\tilde{\Lambda}$ at the 10–20% level [61, 62].

Future observations of tidal deformabilities from binary mergers, especially of low-mass systems, could place tight constraints on whether SQSs are realized in nature.

3.4 Spin Constraints and Angular Momentum

The dimensionless spin parameter $\chi = cJ/(GM^2)$ describes the degree of rotation of a compact object. While many studies focus on mass and radius constraints, the spin properties of SQSs remain underexplored.

Recent work [63] models rotating SQSs with realistic EOSs, showing that:

- SQSs can stably rotate at frequencies up to 1500 Hz, far beyond the fastest known pulsars, with spin parameters approaching $\chi \approx 0.7$.
- The spin limit is not universal but depends on B , Δ , and stellar compactness. Lower B permits more compact configurations that can support higher χ before reaching mass-shedding limits.
- No published studies have systematically mapped $\chi(B, \Delta)$ across parameter space. However, preliminary modeling suggests χ increases with decreasing B , up to a maximum constrained by the Kepler limit and gravitational radiation instabilities.

4 Theoretical and Observational Constraints on Boson Stars

Boson stars (BSs) represent a class of hypothetical compact objects arising as self-gravitating configurations of complex scalar or vector bosonic fields in four-dimensional general relativity. Unlike traditional astrophysical objects composed of fermionic matter, such as neutron stars or white dwarfs, BSs are stabilized by a fundamentally different mechanism: the balance between gravitational attraction and quantum wave effects inherent to bosons. Over the past decades, the properties of these objects—including their mass, spin, and stability—have been extensively explored through analytical methods and numerical simulations, yielding a rich theoretical understanding [64–66].

BSs emerge as solutions to the coupled Einstein-Klein-Gordon or Einstein-Proca field equations, describing complex scalar or vector fields minimally coupled to gravity. The interplay between the boson mass m_b , self-interactions, and gravitational effects gives rise to a diverse spectrum of solutions ranging from dilute, weakly bound states to highly compact configurations that can rival neutron stars in density and gravitational field strength.

4.1 Fundamental Properties and Mass Scaling

In the simplest scenario, where bosons are treated as free fields without self-interactions, BSs possess a characteristic maximum mass M_{\max} determined by the boson mass and the Planck scale, following the well-known scaling law [67]:

$$M_{\max} \sim \frac{M_{\text{Pl}}^2}{m_b}, \quad (4.1)$$

where M_{Pl} denotes the Planck mass. This inverse dependence on the boson mass indicates that lighter bosons can form more massive BSs, suggesting intriguing astrophysical relevance if ultra-light bosonic particles (e.g., axion-like particles) exist.

However, the free-field case represents a simplified picture. Realistic bosonic fields can exhibit self-interactions, modeled through nonlinear potentials that drastically alter the BS mass and stability profiles. The most studied self-interaction is a quartic term,

$$V(|\Phi|) = m_b^2 |\Phi|^2 + \frac{\lambda}{2} |\Phi|^4, \quad (4.2)$$

where λ parametrizes the interaction strength. In regimes where self-interactions dominate ($\lambda \gg 1$), the maximum mass scales as [66, 68]:

$$M_{\max} \sim \sqrt{\lambda} \frac{M_{\text{Pl}}^3}{m_b^2}, \quad (4.3)$$

significantly exceeding the free-field upper bound. This enhancement implies that self-interacting BSs can potentially attain astrophysical masses comparable to compact stars or black holes, thereby increasing their viability as astrophysical objects or dark matter candidates [69].

Beyond quartic potentials, more complex self-interactions such as solitonic potentials,

$$V(|\Phi|) \sim \left(1 - e^{-|\Phi|^2}\right), \quad (4.4)$$

have been explored, revealing even richer phenomenology and stability features [70].

4.2 Rotating Boson Stars: Angular Momentum Quantization and Structure

Rotation introduces additional complexity and novel phenomena in BS configurations. Unlike classical rotating fluid stars, rotating BSs possess angular momentum that is discretely quantized. The bosonic field is endowed with a harmonic azimuthal dependence,

$$\Phi(t, r, \theta, \phi) = \psi(r, \theta) e^{i(m\phi - \omega t)}, \quad (4.5)$$

where $m \in \mathbb{Z}$ is the azimuthal quantum number. This quantization leads to discrete angular momentum values,

$$J = mN, \quad (4.6)$$

with N the total particle number [64]. Such a quantum feature is absent in classical rotating stars and black holes, highlighting the fundamentally quantum nature of BSs.

Rotating BSs typically exhibit toroidal energy density distributions, as opposed to the spherical symmetry of non-rotating configurations. This geometry affects stability and gravitational field multipolarity [71, 72]. Self-interactions further influence the range of stable spinning configurations, often broadening the parameter space where rotation can be sustained without collapse or dispersion [72, 73].

4.3 Deviations from Black Hole Geometries

Although BSs are gravitationally compact, their spacetime geometry deviates notably from the Kerr solutions describing rotating black holes. One prominent difference lies in the multipole moments, such as the quadrupole moment, which scale differently compared to Kerr black holes [72]. These deviations have observational consequences, for instance, in gravitational wave signals from inspiraling binaries or in the orbital dynamics of nearby test particles.

4.4 Astrophysical and Cosmological Implications

The unique mass-spin relations and the potentially ultra-light boson mass scales open avenues for BSs as dark matter candidates, gravitational wave sources, and exotic compact objects capable of mimicking black holes without event horizons. Notably, BSs composed of ultra-light bosons with masses around $m_\phi \sim 10^{-22} \text{eV}$, can form structures with masses as low as $\sim 10^{-10} M_\odot$, comparable to planetary masses. This ultra-light regime connects BSs to models of fuzzy dark matter, where wave-like quantum effects shape galactic structure [65].

5 Lower Mass Limits of Neutron Stars

Neutron stars arise from the gravitational collapse of massive stellar cores, stabilized by neutron degeneracy pressure and nuclear interactions. The lower mass limit of stable neutron stars is determined by the interplay between the EOS stiffness and cooling dynamics during

the proto-neutron star phase. Theoretical models and numerical solutions to the Tolman-Oppenheimer-Volkoff (TOV) equations indicate that the **absolute lower mass limit** for a cold, stable neutron star is approximately $0.1 - 0.2M_\odot$ [74, 75].

At sub-threshold masses, neutron degeneracy pressure becomes insufficient to counteract gravitational collapse, causing further contraction towards either a white dwarf or a different compact object class. Additional studies suggest that proto-neutron stars, which originate as lepton-rich remnants of supernovae, may have higher minimum mass limits of around $1.0M_\odot$ due to the thermal energy and trapped neutrino contributions during the early post-collapse stage [74].

Variations in neutron star mass-radius diagrams arise from EOS differences, particularly in models incorporating hyperon populations, strange baryons, or other exotic phases of dense matter [76]. Low-mass neutron stars with softer EOS exhibit larger radii for a given mass, making them distinguishable from more compact strange quark stars.

6 Primordial Black Holes

Primordial black holes (PBHs) are hypothetical black holes formed in the early Universe, long before the formation of the first stars or galaxies. They are expected to arise from the direct gravitational collapse of large density fluctuations generated during or shortly after inflation, or from other early-Universe processes such as phase transitions or the collapse of cosmic strings [77, 78]. Unlike astrophysical black holes, whose masses are set by stellar evolution channels and limited by the TOV bound for neutron stars, PBHs are not subject to baryonic physics constraints. Their possible mass spectrum thus spans an enormous range, from sub-planetary masses up to many solar masses, determined primarily by the cosmological horizon mass at their time of formation [79, 80].

The potential existence of PBHs is of significant interest for both cosmology and fundamental physics. PBHs have been considered viable candidates for (a fraction of) dark matter [77, 81], and their merger rates could contribute to the binary black hole population observed by current gravitational-wave detectors [82]. In particular, the detection of a sub-solar mass black hole ($M \lesssim 1 M_\odot$) would provide a striking signature of primordial origin, as there are no known astrophysical channels capable of producing such light black holes [83, 84].

From a gravitational-wave perspective, a crucial property of PBHs is that, as vacuum solutions of general relativity without any internal matter structure, they possess strictly vanishing tidal deformability. The dimensionless tidal Love number of a black hole in classical general relativity is exactly zero, $k_2 = 0$ [5, 85, 86]. As a result, PBHs do not leave significant tidal imprints in the late inspiral gravitational waveform of a binary merger. This provides a clean theoretical baseline against which other compact objects—such as neutron stars [4, 87] or exotic compact objects like strange quark stars [6, 8] and boson stars [88]—can be discriminated. Any confident detection of nonzero tidal deformability for a sub-solar mass compact object would strongly disfavor a PBH interpretation.

PBH spin predictions are more model-dependent than their masses. In many scenarios—particularly for PBHs formed during radiation domination—the expected spins are low, since initial overdensities are nearly spherical and angular momentum is largely washed out by pressure gradients [89]. However, PBHs formed during a matter-dominated era can acquire significant angular momentum through tidal torques and initial asphericities, potentially reaching high, even near-maximal, dimensionless spin parameters ($\chi \lesssim 1$) at formation [90, 91]. Subsequent accretion and binary evolution may further alter the spin distribu-

tion, but the possibility of rapidly rotating PBHs remains open and could leave observable imprints in the gravitational-wave population.

Combining measurements of mass, spin, and tidal deformability with next-generation detectors such as Cosmic Explorer [92] and the Einstein Telescope [93, 94] will significantly enhance our ability to distinguish PBHs from astrophysical black holes or other exotic compact objects. In particular, third-generation sensitivities will allow for detections of sub-solar mass PBHs out to cosmological distances, opening a unique observational window into early-Universe physics and the possible primordial origin of black holes.

7 Methods and Assumptions

The results are significantly dependent on the network of detectors considered. In this work, we consider a standard 3G network composed of 10 km arm-length triangular ET in Sardinia, plus two CE, one of 40 km arm-length in the US and one of 20 km arm-length also in the US. For more information on the detectors, see appendix A. One of the improvements that the FIM analysis can bring is that we do not have to limit the analysis to a few sources. In fact, in each cell of the figures shown, we plot the median maximum redshift calculated from a small catalog of twenty sources. These catalogs, obtained by uniformly sampling the extrinsic parameters (i.e., inclination, sky position, polarization angle, and phase and time of coalescence), were created to partially reduce the noise associated with a single realization. For each event, we obtain an estimate of the maximum redshift for a 3σ detection using a bisection method; subsequently, we take the median of the twenty redshift estimates. This leads to $\mathcal{O}(1 - 5 \times 10^5)$ FIM evaluation per plot. The code used for the evaluation is `GWJulia` [32], which enabled a very fast evaluation of the FIMs, making it feasible to run all the FIMs required for this work on a laptop.

We now proceed with setting up the Fisher Matrix evaluation, and an important question in each scenario is the waveform choice. We use the most advanced waveform at our disposal, given the physical constraints, since the computation time is not a significant issue for FIM analysis¹. In this work, we analyze different scenarios and summarize the information on the waveforms in table 1 and in table 2. For each waveform, in the `GWJulia` implementation, we use settings replicating the default options of `LALSuite` [96], e.g., the frequency where to cut the waveform. The waveforms used in this work are `IMRPhenomXAS` [97] for the BBH case, `IMRPhenomD_NRTidal_v2` [98–100] for the BNS case, `IMRPhenomNSBH` [101, 102] for the NSBH case, and `TaylorF2` [103–105] when working outside the calibration ranges.

The tidal deformability used for NS is obtained using the AP3 EOS [106], with the TOV solver provided by `LALSuite` [96]. This EOS is compatible with the current constraints, in particular the one provided by GW170817 [11, 57]. For more information on the EOS used in this work, we refer to appendix A.

For the BS tidal deformability, we consider a phenomenological approach, i.e., for each mass M we do not fix the boson mass m_b . Instead, we consider a BS which is softer than a NS, choosing the tidal deformability to follow the AP3 EOS slope but with a five times larger magnitude. This allows us to place more competitive bounds on the tidal deformability of BS, since softer BS will have an even larger signature, without the need to focus on a single boson mass, m_b or potential shape.

¹`GWJulia` has also the possibility of adding higher order harmonics for the BBH case [95]; we reserve the option to add this in future work.

object 1/ object 2	PBH	NS	ECO
NS	TaylorF2	IMRPhenomD_Tidal	TaylorF2
BH	IMRPhenomXAS	IMRPhenomNSBH	TaylorF2
ECO	/	/	TaylorF2

Table 1. Table representing which waveform model is used in the different scenarios. The criterion for the choice is to use the most advanced waveform given the physical requirements. `IMRPhenomD_Tidal` stands for `IMRPhenomD_NRTidal_v2`

waveform	q	$M_2 [m_\odot]$	χ_1	χ_2	Λ
IMRPhenomD_NRTidal_v2	[1,3]	[1,3]	[-0.6,0.6]	[-0.6,0.6]	[0,5000]
IMRPhenomXAS	[1, 1000]	BBH	[-0.9,0.9]	[-0.9,0.9]	0.
IMRPhenomNSBH	[1,15]	[1,3]	[-0.5,0.5]	0.	[0,5000]

Table 2. Summary of the calibration regimes of validity of the different waveforms used. Note that the [1,1000] for `IMRPhenomXAS` is the calibration range claimed in [97]

8 Results

In fig. 1, we show the maximum redshift at which a 3σ measure of a sub-solar mass PBH is possible in a merger with a neutron star (NS) of varying masses. Therefore we show the redshift $z_{3\sigma}$ such that

$$m_{\text{PBH}} + 3\sigma(z_{3\sigma}) < 1M_\odot \quad (8.1)$$

The waveform used is `TaylorF2`, which includes leading-order tidal effects but lacks merger and ringdown information—resulting in a conservative estimate of the sensitivity. The panels depict three spin configurations: low spins, high spin of the PBH and high aligned spins of both bodies. Spins have a modest impact on the inspiral phase, so we find very weak modifications in the different configurations. The optimal configuration is reached for $M_{\text{NS}} \sim 2.1 M_\odot$ and $M_{\text{PBH}} \sim 0.5 M_\odot$, with the median horizon redshift extending beyond $z \sim 1$. This highlights the importance of heavy neutron star companions in maximizing the reach of PBH identification.

In fig. 2, we consider instead mergers of a sub-solar mass PBH with a stellar black hole companion and we still examine 3σ sub-solar detection. This time, we use the `IMRPhenomXAS` waveform to account for high mass ratios. Three spin configurations are again analyzed, showing a more pronounced effect from the high spins alignment compared to the NS case, due to the inclusion of the merger in the evaluation. The maximum redshift is attained for BH mass $M_{\text{BH}} \sim 40 M_\odot$ and PBH masses around $M_{\text{PBH}} \sim 0.4 M_\odot$, reaching beyond $z \sim 3$. The left panel (low spins) shows the lowest redshift contours, while the right panel (high aligned spins) demonstrates the highest detection reach. The dashed contour denotes the threshold beyond which the mass ratio $q > 50$. The choice of such a threshold is strongly dependent on the goals of the analysis. E.g., in the context of Bayesian parameter estimations, similar thresholds are put in place; however, this choice is a complex topic, dependent on the waveform model, the spins, and total mass of the event [107–110]. In this work, we consider events inside the full calibration range of `IMRPhenomXAS` [97]. Beyond $q > 1000$, shown in white, the waveform lies outside the calibration range. This plot confirms that high-mass, high-spin BH companions enable the deepest reach for sub-solar PBHs.

Fig. 3 displays the same detection calculation for a strange quark star (SQS) as the low-mass companion, assuming the SQM3 EOS [111]. Results are shown for NS-SQS and BH-SQS

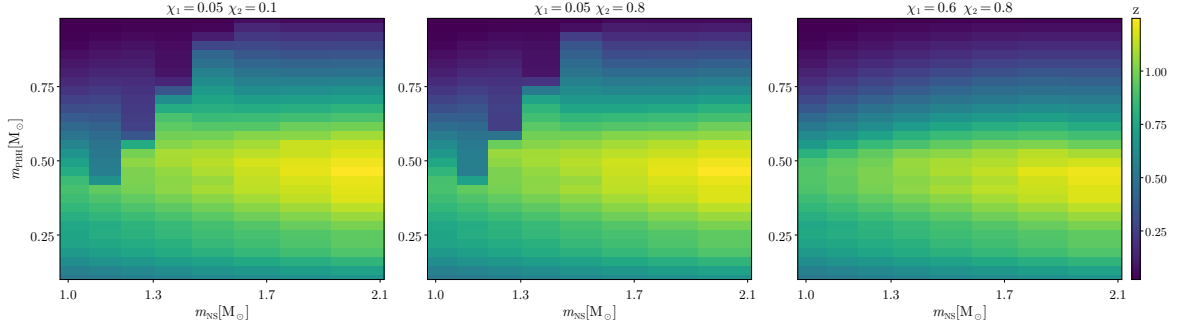


Figure 1. In these figures, we show the maximum redshift at which we can have a 3 sigma measurement of a sub-solar mass PBH, in the case where the merging partner is a *neutron star*. The first mass, on the x -axis, is a NS, while the PBH masses are on the y -axis. The different plots represent different spin configurations: low-spins (*left*), high PBH spin (*center*) and high aligned spins (*right*). The waveform used is TaylorF2 and each pixel represents the median redshift of 20 events. The largest redshift is reached for the heaviest NS considered ($M_{\text{NS}} \sim 2.1 M_{\odot}$) in combination with a PBH of mass $m_{\text{PBH}} \sim 0.5 M_{\odot}$.

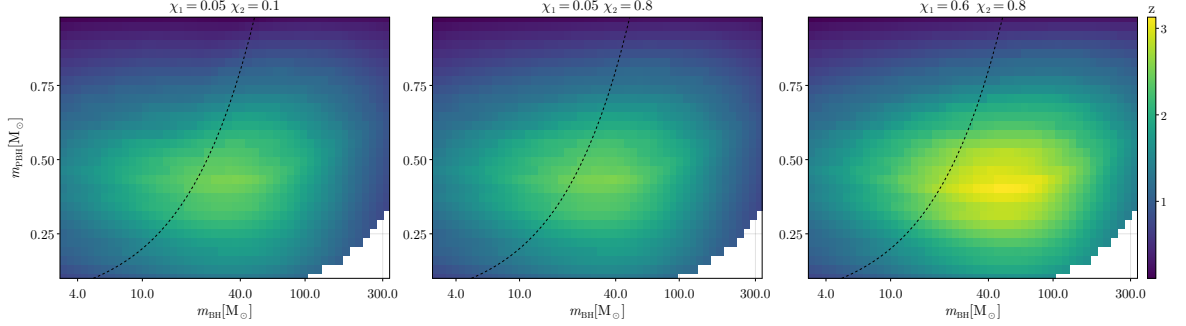


Figure 2. In these figures, we show the maximum redshift at which we can have a 3 sigma measurement of a sub-solar mass BH, in the case where the merging partner is a *black hole*. The first mass, on the x axis, is a BH, while the PBH masses are on the y -axis. The different plots represent different spin configurations: low-spins (*left*), high PBH spin (*center*) and high aligned spins (*right*). The waveform used is IMRPhenomXAS and each pixel represents the median redshift of 20 events. The largest redshift is reached for $M_{\text{BH}} \sim 40 M_{\odot}$ in combination with a PBH of mass $m_{\text{PBH}} \sim 0.4 M_{\odot}$. The presence of high BH spin slightly enlarges the mass of the BH at which this maximum occurs. Moreover, both high-spin configurations lead to significantly larger median redshifts across all masses considered. The dashed lines indicate where the mass ratio $q = 50$; above the lines, the waveform is highly reliable; in the white region, $q > 1,000$ and the waveform lies outside the calibration range.

systems and we evaluate only the low spin configuration ($\chi_1 = 0.05$, $\chi_2 = 0.1$). The trends are similar to those in the PBH case, with detection optimized for heavy companions and light SQSs (down to $0.3 - 0.4 M_{\odot}$). However, these plots only reflect sub-solar mass detectability; distinguishing SQSs from PBHs requires measurement of nonzero tidal deformability, which remains inaccessible at such high redshifts. Thus, this figure sets bounds on the regime where exotic self-bound objects could be confused with PBHs.

In fig. 4, we perform an analogous analysis for boson star (BS) companions. We assume an EOS yielding a tidal deformability $\Lambda = 5 \times \Lambda_{\text{AP3}}$ to amplify possible differences from PBHs. Also, here we evaluate only the low spin configuration ($\chi_1 = 0.05$, $\chi_2 = 0.1$). Even under this

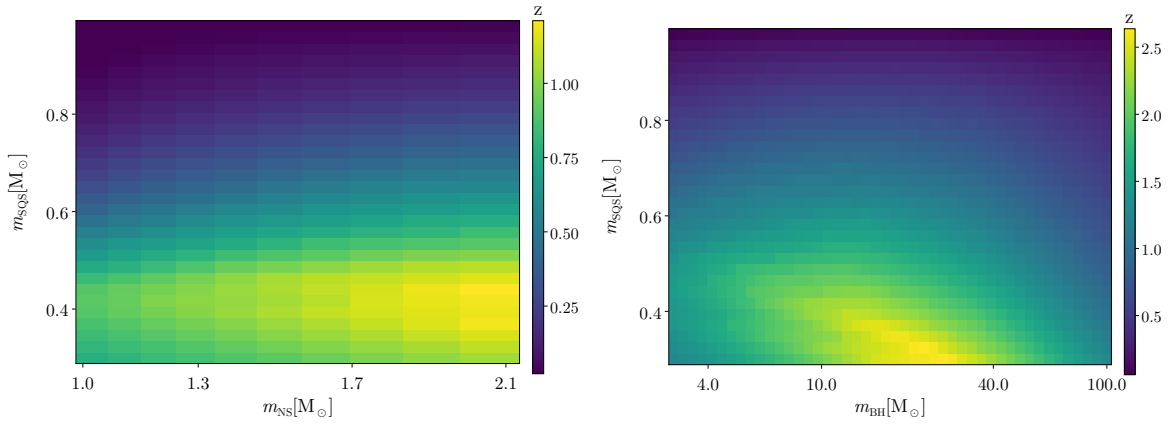


Figure 3. Maximum redshift at which a 3 sigma measurement of sub-solar mass is possible, for a SQM3 EOS. We consider the **TaylorF2** waveform model. Object 1 is a NS in the *left* panel and a BH in the *right* panel. These plots do not imply the ability to distinguish between a SQS and a PBH, as the tidal deformability at these redshifts is poorly constrained. The maximum redshift for a merger with the NS is found at the point $\sim (2.1, 0.4)M_\odot$, while for the merger with BH the point is at $\sim (30, 0.3)M_\odot$.

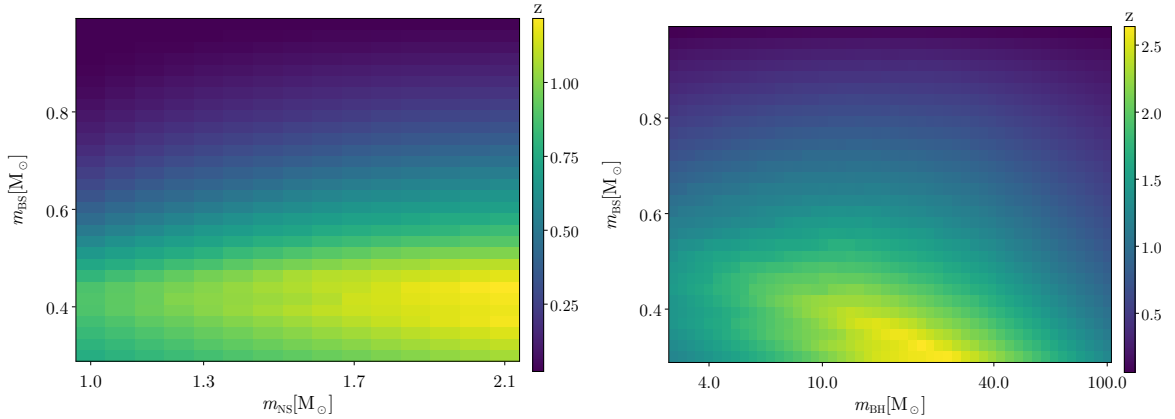


Figure 4. Maximum redshift at which we can have a 3 sigma measurement of sub-solar mass for a BS EOS. We consider an EOS producing a tidal deformability of 5 times the AP3 EOS, with the boson mass adapted accordingly. We considered the **TaylorF2** waveform model. Object 1 is a NS in the *left* panel and a BH in the *right* panel. Again, these plots do not imply distinguishability from a PBH via tidal deformability imprints. The maximum redshift for a merger with the NS is found at the point $\sim (2.1, 0.4)M_\odot$ while for the merger with BH the point is at $\sim (30, 0.3)M_\odot$.

optimistic assumption, the tidal signature is too small to affect detectability at cosmological distances. More significant differences could be expected by using a full inspiral-merger-ringdown waveform, designed for BS [112]. The maximum redshift for detection again lies near the $(2.1, 0.4)M_\odot$ point for NS-BS systems and around $(30, 0.3)M_\odot$ for BH-BS systems, consistent with the SQS and PBH trends.

The prospect of using the Love numbers to distinguish the nature of the compact objects is quantified in fig. 5 when the first object is a NS, while fig. 6 deals with the BH case. Concerning the first case, we can picture the situation in which an unknown second body merges

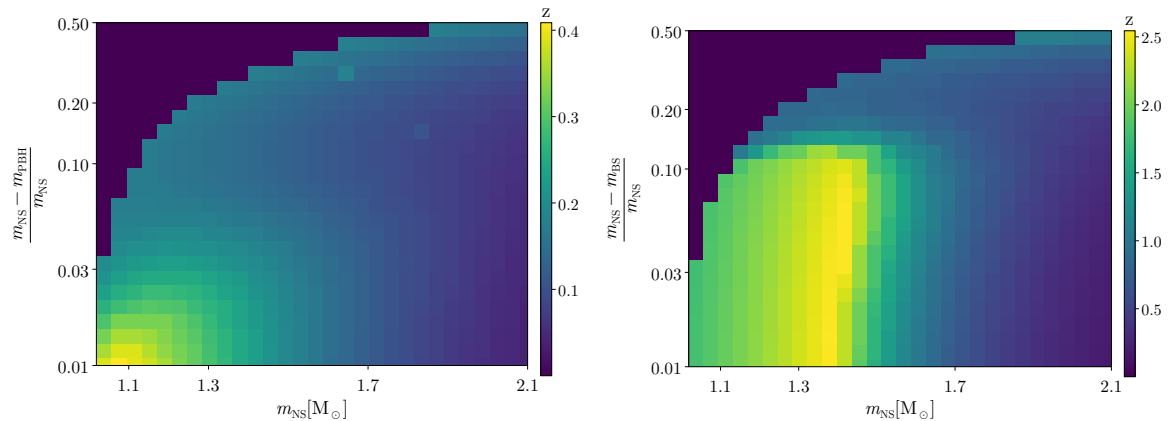


Figure 5. Maximum redshift at which we can have a 3 sigma exclusion of PBH (*left*) or BS (*right*) using tidal effects. The injected signal is a BNS merger, using `IMRPhenomD_NRTidal_v2`. We constrain the tidal parameter of the second NS Λ_2 after conditioning over the first tidal parameter Λ_1 . We limit ourselves to objects larger than a solar mass and on the y axis, we plot the relative difference of the two objects. The best constraints are for light NS of similar masses $\sim (1.1, 1.1)M_\odot$ in the PBH case, while for the BS case, it is at $\sim (1.4, 1.3)M_\odot$.

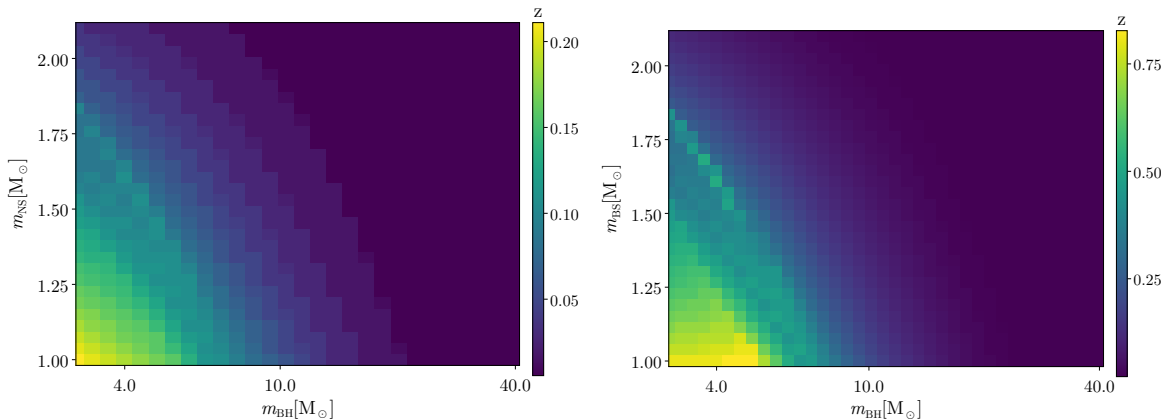


Figure 6. Same plot as before in the case of a BH as the first object. The second object is a NS and the waveform used is `IMRPhenomNSBH`. We limit ourselves to masses greater than a solar mass. As before, we constrain the maximum redshift at which we can have a 3σ exclusion of the tidal deformability Λ of a PBH (*left*) or BS (*right*). Also in this case, the best constraints are for light objects of similar masses $\sim (3, 1)M_\odot$ in the PBH case, while for the BS case, it is at $\sim (4, 1)M_\odot$.

with a NS, and we constrain the nature of this second body using its tidal deformability. We explore masses larger than $1 M_\odot$, and we show on the y axis the relative mass difference. Using the FIM formalism, we generate a BNS signal, using `IMRPhenomD_NRTidal_v2`. Then we extract the error on the tidal deformability Λ_2 and compute the maximum redshift at which we can reject the PBH hypothesis (*left*) or the BS hypothesis (*right*) with a 3σ confidence interval. An important assumption is that we condition on the tidal deformability of the first NS Λ_1 . This assumes that we have some outside knowledge of the first body, e.g., astronomical observation, or enough knowledge of the EOS of NS to condition on it. We are projecting these results for 3G detectors, so our current understanding of EOS could

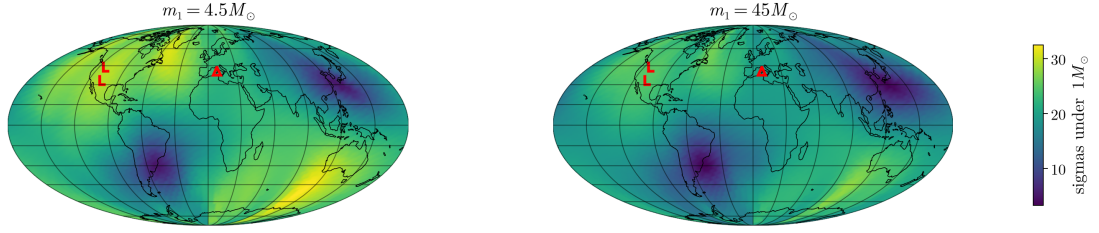


Figure 7. Number of sigmas for a subsolar detection of a PBH. The plots show the detector frame, i.e., a frame in which we observe the sky rotating with a period of one day. The detectors used are represented by red signs, L's for the two CE and Δ for the triangular ET. The event chosen has a PBH mass $m_{\text{PBH}} = 0.3M_{\odot}$ and a primary mass of $m_{\text{BH}} = 4.5M_{\odot}$ (*left*) and $m_{\text{BH}} = 45M_{\odot}$ (*right*). The sky location leads to largely different results spanning from a $\sim 3 - 4$ sigma measurement to a more than 30 sigma measurement.

change drastically in the meantime. Concerning the results, the tidal effects are discernible for $z \lesssim 0.4$, with $\sim 3\sigma$ significance in the most favorable part of the parameter space, which corresponds to masses $\sim (1.1, 1.1)M_{\odot}$ in the PBH case. In the right panel, we reject a BS with $\Lambda = 5 \times \Lambda_{\text{AP3}}$, extending the detection range to $z \sim 2.5$, for masses $\sim (1.4, 1.3)M_{\odot}$. This happens because the BS considered are significantly deformable, leading to optimistic constraints using our setup. The picture changes significantly if we remove the conditioning on the first tidal parameter, due to the large correlation of the two tidal deformations. In this case, a better constraint could be obtained on the combination $\tilde{\Lambda}$.

In fig. 6, we follow the same procedure as before, with the important difference that the first object is a BH and no conditioning is performed. The waveform used is **IMRPhenomNSBH** and we look for a 3σ exclusion of a PBH Hypothesis (*left*) and BS (*right*). The best constraints are achieved for small mass BHs and small mass NSs, masses $\sim (3, 1)M_{\odot}$ in the PBH case, while for the BS case, it is at $\sim (4, 1)M_{\odot}$. Thus, this figure illustrates a key limitation: while mass-based PBH identification is viable at cosmological distances, tidal discrimination is restricted to the local Universe, unless some additional information can be incorporated to perform the conditioning procedure followed in fig. 5.

The influence of sky position on sub-solar mass detection is presented in fig. 7. For a fiducial PBH mass of $0.3M_{\odot}$ and BH companions of $4.5M_{\odot}$ (*left*) and $45M_{\odot}$ (*right*), we observe dramatic variations in detection significance due to the directional sensitivity of the 3G detector network. At best, over 30σ detection is possible; at worst, significance dips to $\sim 3\sigma$, indicating that the significance of a future detection will be heavily influenced by the sky position. The redshift used for the left panel event is $z = 0.65$ and the two events have similar SNR ~ 10 after being averaged over the sphere.

Sky-position effects for tidal detectability are shown in fig. 8 and we reproduce the procedure used for fig. 5. The statistical significance of detecting $\Lambda_2 > 0$ hovers between 1σ and 2σ , depending on the sky position. The angular modulation resembles that seen in sub-solar mass detection but with lower overall SNR, reinforcing the challenge of leveraging tidal measurements for PBH exclusion.

Finally, fig. 9 summarizes PBH detection prospects in terms of expected event rates and redshift reach. We solely consider mergers of stellar black holes (whose mass is on the x axis) with primordial black holes (y axis). For the former, we adopt the stellar black hole mass function recently modeled by Sicilia et al. [113], which computes an ab initio relic distribution

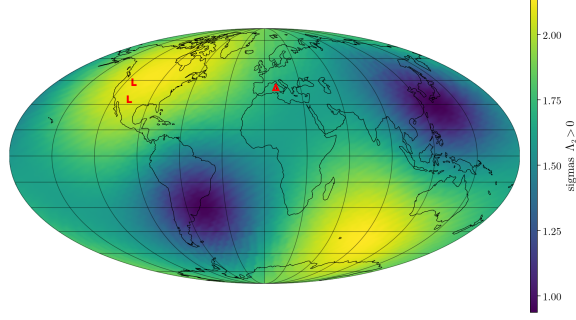


Figure 8. Number of sigmas to claim a $\Lambda_2 > 0$. The events are BNS obtained with IMRPhenomD_NRTidal_v2 and we follow the same procedure detailed before, i.e., we condition on the tidal deformability of the first NS Λ_1 . In this case, there is a less significant difference with respect to fig. 7 in the number of sigmas achieved in different parts of the sky, ranging in $\sim [1, 2]\sigma$. The results resemble those of fig. 7 with a significant smearing of its sharper feature.

using the SEVN stellar/binary evolution code alongside galaxy formation prescriptions; for the PBH abundance, we instead assume, for a given PBH mass, the maximal-possible abundance of PBHs, i.e., we maximize f_{PBH} , for a monochromatic mass function, using the constraints of Ref. [114, 115]. The merger rate functional form we employ follows an analytic estimate of the fitting expression provided in Ref. [116], suitable for phenomenological studies. The dips visible between PBH masses of 0.3 and 1 solar masses are due to the constraints on the PBH abundance $f_{\text{PBH}}(M_{\text{PBH}})$ in that mass range.

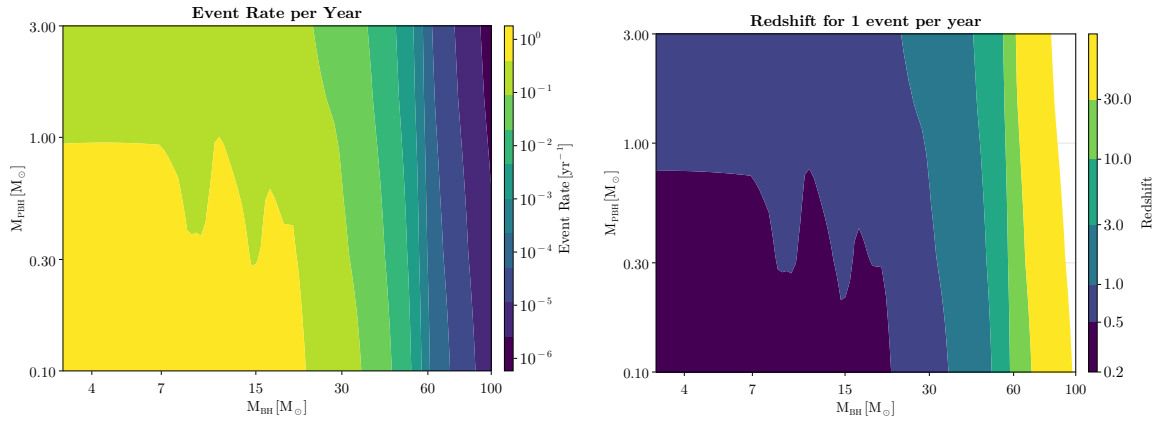


Figure 9. Event rate within a one Gpc radius sphere (*left*) and redshift corresponding to one event per year (*right*) of stellar BH vs PBH. Lighter mergers are preferred and, importantly, most of the interesting parameter space from fig. 2 has at least one event a year.

The left panel shows contours of 1 event/year across the plane of stellar-mass PBH vs light PBH. The right panel translates this into redshift, showing that mergers between, e.g., $30 M_\odot$ and $0.3 M_\odot$, which was the most favourable configuration in fig. 2 can be detected up to once a year. These figures define the observational frontier for probing early-Universe black hole populations using third-generation gravitational-wave observatories.

Note that since 1 Gpc approximately corresponds to $z \simeq 0.23 - 0.24$, fig. 9 indicates that in a large swath of parameter space there may be as many as $\mathcal{O}(10)$ events involving a sub-solar mass object where tidal deformability is detectable with 3G detectors.

In conclusion, 3G detectors will offer exceptional reach in identifying sub-solar mass PBHs, with sensitivity extending to redshifts $z \gtrsim 3$ for BH-PBH systems. However, the ability to confirm or rule out their primordial origin based on their null tidal signature is fundamentally constrained by the redshift at which tidal effects become measurable. Only low-redshift, high-SNR events will yield definitive discrimination between PBHs and exotic material compact objects.

9 Discussion and Conclusions

In this work, we have investigated the prospects for identifying sub-solar mass primordial black holes and distinguishing them from possible astrophysical and exotic compact object impostors using third-generation gravitational-wave detectors such as the Einstein Telescope and Cosmic Explorer. Employing the Fisher matrix formalism, we quantified the maximum redshifts at which sub-solar mass companions can be measured with high significance, as well as the redshift ranges where tidal deformability measurements could exclude the primordial black hole hypothesis.

Our analysis shows that sub-solar mass primordial black holes, if present in binary systems with neutron stars or stellar-mass black holes, will be detectable out to cosmological distances. In particular, we find that black hole–primordial black hole binaries can be observed up to redshift $z \gtrsim 3$, and in some configurations even farther, while neutron star–primordial black hole binaries are typically detectable out to redshift $z \sim 1$. These results establish that third-generation detectors will have the sensitivity required to probe sub-solar primordial black holes well beyond the capabilities of the current LIGO–Virgo–KAGRA network.

A central challenge, however, lies in establishing the nature of the detected low-mass compact objects. While primordial black holes are characterized by vanishing tidal deformability ($k_2 = 0$), neutron stars, strange quark stars, and boson stars exhibit finite tidal signatures that depend on their respective equations of state. We have shown that tidal measurements, though in principle decisive, are restricted to the local Universe: even with third-generation sensitivity, confident exclusion of the primordial black hole hypothesis through detection of non-zero tidal effects is possible only for redshifts $z \lesssim 0.3\text{--}0.5$, depending on the equation of state and binary configuration. This implies that while mass-based identification of sub-solar objects as primordial black holes can be achieved at high redshift, tidal-based discrimination between primordial black holes and material impostors is fundamentally limited to nearby events.

Our results highlight a dual observational frontier. On the one hand, cosmological reach for sub-solar mass detections offers unprecedented opportunities to map the primordial black hole parameter space, probe early-Universe physics, and test the hypothesis that primordial black holes constitute a fraction of the dark matter. On the other hand, the limited redshift horizon for tidal discrimination underscores the importance of low-redshift, high signal-to-noise events for definitively ruling out non-primordial interpretations. This complementarity suggests that robust population-level inference strategies—combining mass spectra, spin distributions, event rates, and tidal signatures—will be essential for establishing the primordial origin of light black holes.

The analysis presented here relies on several simplifying assumptions, including the use of phenomenological prescriptions for strange quark star and boson star equations of state, waveform models calibrated within limited mass-ratio regimes, and the Fisher matrix approximation. Future work should refine these aspects, for instance by employing Bayesian parameter estimation with full inspiral–merger–ringdown waveforms tailored to exotic compact objects, by incorporating more realistic population models of primordial black holes and exotic compact objects, and by exploring synergies with electromagnetic and cosmological probes.

In conclusion, we find that third-generation gravitational-wave observatories will provide a decisive test on the existence of sub-solar primordial black holes. The detection of a sub-solar mass black hole would be a striking signal of new physics, strongly indicative of a primordial origin. Conversely, detection of finite tidal effects in the same mass range would point toward the realization of exotic states of matter, such as strange quark matter or bosonic condensates. Either outcome would have profound implications for nuclear physics, particle physics, and cosmology, reinforcing the role of gravitational waves as a unique tool for exploring the deep connections between astrophysics and fundamental physics.

A Technical details

A.1 Detectors

The positions and orientations of the detectors are reported in table 3 while their power spectral densities (PSD) are plotted in the *left* panel of fig. 10.

	Latitude	Longitude	Orientation
CE 40 km	43.83	-112.82	-45.0
CE 20 km	33.16	-106.48	-105.0
ET 10 km triangular	40.52	9.42	0.0

Table 3. Latitude, longitude and orientation with respect to the local East of the three detectors used in this work.

A.2 Tidal deformabilities

The mass of the bosonic constituent m_b sets the fundamental mass and length scales of a boson star, with the maximum mass scaling as $M_{\max} \sim M_{\text{Pl}}^2/m_b$ and the typical radius $R \sim (Gm_b^2 M)^{-1}$ [67, 117]. The effective EOS arises from the scalar potential: for free bosons the pressure–density relation is entirely determined by the field configuration, while with quartic self-interactions, $V(\phi) = \frac{\lambda}{4}|\phi|^4$, one can approximate a polytropic form $p \sim (\lambda/4m_b^4)\rho^2$ [66]. Given an assumed EOS, the mass–radius relation $M(R)$ is fixed, and thus the compactness $C = GM/R$, which controls the dimensionless tidal deformability $\Lambda = \frac{2}{3}k_2 C^{-5}$, with k_2 the Love number [118]. Lighter bosons generically lead to extended, low-compactness configurations with large Λ , while heavier bosons or strongly self-interacting fields yield more compact stars with suppressed tidal signatures, potentially compatible with gravitational-wave constraints from events such as GW170817 [119]. In our study, we do not impose any theoretical priors on λ and m_b and the resulting microphysics, but rather assume a phenomenological EOS. In fig. 10, we show the three EOS used in this work. The SQM3 tidal deformability [120] is similar to the AP3 one, with the significant difference that SQM3 has

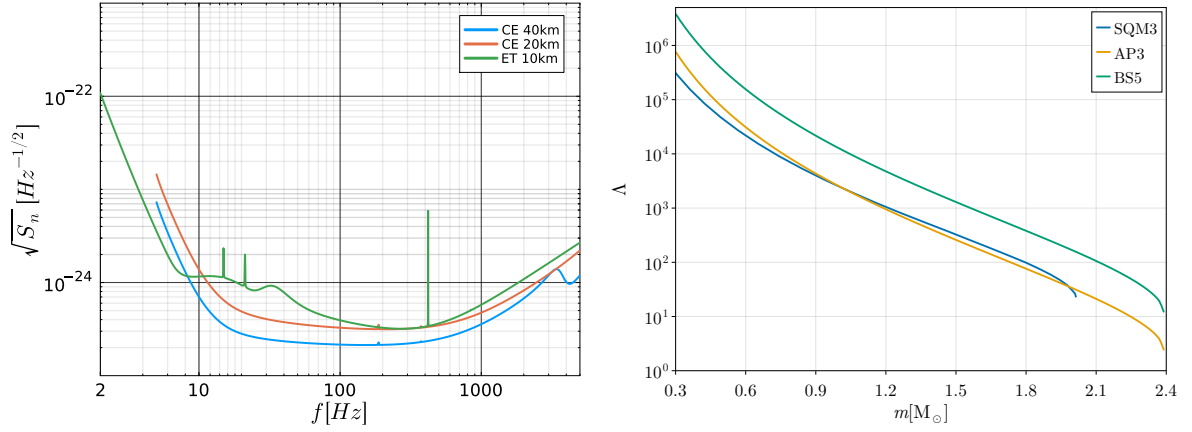


Figure 10. *Left:* PSD of the three detectors used in this work, one L-shape Cosmic Explorer with 40 km arm lengths (blue), one L-shape Cosmic Explorer with 20 km arm lengths (orange) and a triangular Einstein Telescope with 10km arms (green)

Right: Relations of mass of the compact object m and their tidal deformability Λ for a strange quark star SQM3 (blue), for a neutron star with EOS AP3 (orange) and for the phenomenological boson star model employed in this work BS5 (green).

a maximum mass $M_{\max} \sim 2 M_\odot$, while for AP3 $M_{\max} \sim 2.4 M_\odot$. As said in the main text, the BS5 curve reproduces five times the deformability of a AP3 tidal deformability.

Acknowledgments

This work is partly supported by the U.S. Department of Energy grant number de-sc0010107 (SP). AB is supported by ICSC – Centro Nazionale di Ricerca in High Performance Computing, Big Data and Quantum Computing, funded by European Union – NextGenerationEU”. AB would like to thank Stefano Anselmi, Mauro Pieroni, Alessandro Renzi and Angelo Ricciardone for early discussions on the project. AB would like to thank Juan Garcia-Bellido and Sachsa Husa for useful discussions. The authors would also like to thank Liam Colombo Murphy for the strange quark stars EOS solver.

References

- [1] KAGRA, VIRGO, LIGO SCIENTIFIC collaboration, *GWTC-3: Compact Binary Coalescences Observed by LIGO and Virgo during the Second Part of the Third Observing Run*, *Phys. Rev. X* **13** (2023) 041039 [[2111.03606](#)].
- [2] LIGO SCIENTIFIC, VIRGO, KAGRA collaboration, *Tests of General Relativity with GWTC-3*, [2112.06861](#).
- [3] LIGO SCIENTIFIC, VIRGO collaboration, *GW170817: Observation of Gravitational Waves from a Binary Neutron Star Inspiral*, *Phys. Rev. Lett.* **119** (2017) 161101 [[1710.05832](#)].
- [4] S. Postnikov, M. Prakash and J.M. Lattimer, *Tidal love numbers of neutron and self-bound quark stars*, *Phys. Rev. D* **82** (2010) 024016.
- [5] T. Binnington and E. Poisson, *Relativistic theory of tidal Love numbers*, *Phys. Rev. D* **80** (2009) 084018 [[0906.1366](#)].

- [6] F. Crescimbeni, G. Franciolini, P. Pani and A. Riotto, *Can we identify primordial black holes? Tidal tests for subsolar-mass gravitational-wave observations*, *Phys. Rev. D* **109** (2024) 124063 [[2402.18656](#)].
- [7] V. De Luca, G. Franciolini and A. Riotto, *Flea on the elephant: Tidal Love numbers in subsolar primordial black hole searches*, *Phys. Rev. D* **110** (2024) 104041 [[2408.14207](#)].
- [8] E.-P. Zhou, X. Zhou and A. Li, *Constraints on interquark interaction parameters with GW170817 in a binary strange star scenario*, *Phys. Rev. D* **97** (2018) 083015 [[1711.04312](#)].
- [9] Z. Miao, J.-L. Jiang, A. Li and L.-W. Chen, *Bayesian Inference of Strange Star Equation of State Using the GW170817 and GW190425 Data*, *Astrophys. J. Lett.* **917** (2021) L22 [[2107.13997](#)].
- [10] J. Vines and É. Flanagan, *Post-1-newtonian tidal effects in the gravitational waveform from binary inspirals*, *Phys. Rev. D* **83** (2011) 084051.
- [11] C. Pacilio, A. Maselli, M. Fasano and P. Pani, *Ranking Love Numbers for the Neutron Star Equation of State: The Need for Third-Generation Detectors*, *Phys. Rev. Lett.* **128** (2022) 101101 [[2104.10035](#)].
- [12] Z. Ji, J. Chen and G. Wu, *Insights into Neutron Star Matter: EoS Models and Observations*, [2505.05241](#).
- [13] T. Zhao and J.M. Lattimer, *Tidal Deformabilities and Neutron Star Mergers*, *Phys. Rev. D* **98** (2018) 063020 [[1808.02858](#)].
- [14] M. Vaglio, C. Pacilio, A. Maselli and P. Pani, *Bayesian parameter estimation on boson-star binary signals with a coherent inspiral template and spin-dependent quadrupolar corrections*, *Physical Review D* **108** (2023) 023021.
- [15] N. Sennett, T. Hinderer, J. Steinhoff, A. Buonanno and S. Ossokine, *Distinguishing Boson Stars from Black Holes and Neutron Stars from Tidal Interactions in Inspiring Binary Systems*, *Physical Review D* **96** (2017) 024002.
- [16] C. Pacilio, A. Maselli, M. Fasano and P. Pani, *Ranking Love Numbers for the Neutron Star Equation of State: The Need for Third-Generation Detectors*, *Phys. Rev. Lett.* **128** (2022) 101101 [[2104.10035](#)].
- [17] L. Pompili, E. Maggio, H.O. Silva and A. Buonanno, *Parametrized spin-precessing inspiral-merger-ringdown waveform model for tests of general relativity*, *Phys. Rev. D* **111** (2025) 124040 [[2504.10130](#)].
- [18] S. Ghosh and M. Hannam, *On the Identification of Exotic Compact Binaries with Gravitational Waves: a Phenomenological approach*, [2505.16380](#).
- [19] T. Harko and K.S. Cheng, *Maximum mass and radius of strange stars in the linear approximation of the EOS*, *Astron. Astrophys.* **385** (2002) 947 [[astro-ph/0203033](#)].
- [20] X.-L. Zhang, Y.-F. Huang and Z.-C. Zou, *Recent progresses in strange quark stars*, [2404.00363](#).
- [21] J. Takátsy and P. Kovács, *Comment on "Tidal Love numbers of neutron and self-bound quark stars"*, *Phys. Rev. D* **102** (2020) 028501 [[2007.01139](#)].
- [22] N. Uchikata, S. Yoshida and P. Pani, *Tidal deformability and I-Love-Q relations for gravastars with polytropic thin shells*, *Phys. Rev. D* **94** (2016) 064015 [[1607.03593](#)].
- [23] R. Gamba, M. Breschi, S. Bernuzzi, M. Agathos and A. Nagar, *Waveform systematics in the gravitational-wave inference of tidal parameters and equation of state from binary neutron star signals*, *Phys. Rev. D* **103** (2021) 124015 [[2009.08467](#)].

- [24] H. Koehn, T. Wouters, H. Rose, P.T.H. Pang, R. Somasundaram, I. Tews et al., *Probe and Prejudice: Classification of compact objects and model comparison using EOS knowledge*, *Physical Review D* **110** (2024) 103015.
- [25] S.J. Magnall, C. Ecker, L. Rezzolla, P.D. Lasky and S.R. Goode, *Physics-informed Priors Improve Gravitational-wave Constraints on Neutron-star Matter*, *Astrophys. J. Lett.* **988** (2025) L75 [2504.21526].
- [26] C. Huang, *Model-independent Determination of the Tidal Deformability of a $1.4 M_{\odot}$ Neutron Star from Gravitational-wave Measurements*, *Astrophys. J.* **985** (2025) 216 [2505.14822].
- [27] I. Markin, A. Neuweiler, A. Abac, S.V. Chaurasia, M. Ujevic, M. Bulla et al., *General-relativistic hydrodynamics simulation of a neutron star–sub-solar-mass black hole merger*, *Physical Review D* **108** (2023) 064025.
- [28] G. Franciolini, R. Cotesta, N. Loutrel, E. Berti, P. Pani and A. Riotto, *How to assess the primordial origin of single gravitational-wave events with mass, spin, eccentricity, and deformability measurements*, *Phys. Rev. D* **105** (2022) 063510 [2112.10660].
- [29] S. Gasparotto, G. Franciolini and V. Domcke, *Gravitational Wave Memory of Primordial Black Hole Mergers*, **2505.01356**.
- [30] K. Kacanja and A.H. Nitz, *A Search for Low-mass Neutron Stars in the Third Observing Run of Advanced LIGO and Virgo*, *Astrophys. J.* **984** (2025) 61 [2412.05369].
- [31] P. Laskos-Patkos and C.C. Moustakidis, *XTE J1814-338: A potential hybrid star candidate*, *Phys. Rev. D* **111** (2025) 063058 [2410.18498].
- [32] A. Begnoni, S. Anselmi, M. Pieroni, A. Renzi and A. Ricciardone, *Detectability and Parameter Estimation for Einstein Telescope Configurations with GWJulia*, **2506.21530**.
- [33] M. Vallisneri, *Use and abuse of the Fisher information matrix in the assessment of gravitational-wave parameter-estimation prospects*, *Phys. Rev. D* **77** (2008) 042001 [gr-qc/0703086].
- [34] C.L. Rodriguez, B. Farr, W.M. Farr and I. Mandel, *Inadequacies of the Fisher Information Matrix in gravitational-wave parameter estimation*, *Phys. Rev. D* **88** (2013) 084013 [1308.1397].
- [35] L.S. Finn, *Detection, measurement and gravitational radiation*, *Phys. Rev. D* **46** (1992) 5236 [gr-qc/9209010].
- [36] C. Cutler and E.E. Flanagan, *Gravitational waves from merging compact binaries: How accurately can one extract the binary’s parameters from the inspiral wave form?*, *Phys. Rev. D* **49** (1994) 2658 [gr-qc/9402014].
- [37] F. Iacovelli, M. Mancarella, S. Foffa and M. Maggiore, *Forecasting the Detection Capabilities of Third-generation Gravitational-wave Detectors Using GWFAST*, *Astrophys. J.* **941** (2022) 208 [2207.02771].
- [38] U. Dupletsa, J. Harms, B. Banerjee, M. Branchesi, B. Goncharov, A. Maselli et al., *gwfish: A simulation software to evaluate parameter-estimation capabilities of gravitational-wave detector networks*, *Astron. Comput.* **42** (2023) 100671 [2205.02499].
- [39] M. Pieroni, A. Ricciardone and E. Barausse, *Detectability and parameter estimation of stellar origin black hole binaries with next generation gravitational wave detectors*, *Sci. Rep.* **12** (2022) 17940 [2203.12586].
- [40] S. Borhanian, *GWBENCH: a novel Fisher information package for gravitational-wave benchmarking*, *Class. Quant. Grav.* **38** (2021) 175014 [2010.15202].
- [41] S. Borhanian and B.S. Sathyaprakash, *Listening to the Universe with next generation ground-based gravitational-wave detectors*, *Phys. Rev. D* **110** (2024) 083040 [2202.11048].

- [42] J.M.S. de Souza and R. Sturani, *GWDALI: A Fisher-matrix based software for gravitational wave parameter-estimation beyond Gaussian approximation*, *Astron. Comput.* **45** (2023) 100759 [[2307.10154](#)].
- [43] Y. Li, I.S. Heng, M.L. Chan, C. Messenger and X. Fan, *Exploring the sky localization and early warning capabilities of third generation gravitational wave detectors in three-detector network configurations*, *Phys. Rev. D* **105** (2022) 043010 [[2109.07389](#)].
- [44] A. Abac et al., *The Science of the Einstein Telescope*, **2503.12263**.
- [45] PLANCK collaboration, *Planck 2018 results. VI. Cosmological parameters*, *Astron. Astrophys.* **641** (2020) A6 [[1807.06209](#)].
- [46] E. Witten, *Cosmic Separation of Phases*, *Phys. Rev. D* **30** (1984) 272.
- [47] A.R. Bodmer, *Collapsed nuclei*, *Phys. Rev. D* **4** (1971) 1601.
- [48] J.L. Zdunik, *On the mass of moderately rotating strange stars*, *Astron. Astrophys.* **359** (2000) 311 [[astro-ph/0004375](#)].
- [49] G. Lugones and J.E. Horvath, *Color-flavor locked strange matter*, *Phys. Rev. D* **66** (2002) 074017 [[hep-ph/0211070](#)].
- [50] J. Madsen, *How to identify a strange star*, *Phys. Rev. Lett.* **81** (1998) 3311 [[astro-ph/9806032](#)].
- [51] M. Malheiro, E.O. Azevedo, L.G. Nuss, M. Fiolhais and A.R. Taurines, *Small quark stars in the chromodielectric model*, *AIP Conf. Proc.* **631** (2002) 658 [[hep-ph/0111148](#)].
- [52] O.G. Benvenuto and G. Lugones, *The properties of strange stars in the quark mass-density-dependent model*, *Int. J. Mod. Phys. D* **7** (1998) 29.
- [53] L. Paulucci, J.E. Horvath, E.J. Ferrer and V. de la Incera, *Superconducting phases of strange quark matter in the NJL model*, in *Compact Stars in the QCD Phase Diagram III*, 7, 2013 [[1307.2290](#)].
- [54] W.-L. Yuan, A. Li, Z. Miao, B. Zuo and Z. Bai, *Interacting ud and uds quark matter at finite densities and quark stars*, *Phys. Rev. D* **105** (2022) 123004 [[2203.04798](#)].
- [55] H.T. Cromartie and et al., *Relativistic Shapiro delay measurements of an extremely massive millisecond pulsar*, *Nature Astronomy* **4** (2020) 72 [[1904.06759](#)].
- [56] I. Bombaci, G. Lugones and I. Vidana, *Effects of color superconductivity on the nucleation of quark matter in neutron stars*, *Astron. Astrophys.* **462** (2007) 1017 [[astro-ph/0603644](#)].
- [57] LIGO SCIENTIFIC, VIRGO collaboration, *GW170817: Measurements of neutron star radii and equation of state*, *Phys. Rev. Lett.* **121** (2018) 161101 [[1805.11581](#)].
- [58] Z. Liu and Z.-W. Tang, *Probing ultralight isospin-violating mediators at GW170817*, *JHEP* **06** (2024) 090 [[2402.06209](#)].
- [59] Z. Wang, Y. Gao, D. Liang, J. Zhao and L. Shao, *Vetting quark-star models with gravitational waves in the hierarchical Bayesian framework*, *JCAP* **11** (2024) 038 [[2409.11103](#)].
- [60] L. Perot and N. Chamel, *Role of Quark Matter and Color Superconductivity in the Structure and Tidal Deformability of Strange Dwarfs*, *Universe* **9** (2023) 382.
- [61] S.-H. Yang, C.-M. PI, X.-P. Zheng and F. Weber, *Non-Newtonian Gravity in Strange Quark Stars and Constraints from the Observations of PSR J0740+6620 and GW170817*, *Astrophys. J.* **902** (2020) 32 [[1909.00933](#)].
- [62] A. Kumar, V.B. Thapa and M. Sinha, *Compact star merger events with stars composed of interacting strange quark matter*, *Mon. Not. Roy. Astron. Soc.* **513** (2022) 3788 [[2204.11034](#)].

- [63] S. Bhattacharyya, I. Bombaci, D. Logoteta and A.V. Thampan, *Fast spinning strange stars: possible ways to constrain interacting quark matter parameters*, *Mon. Not. Roy. Astron. Soc.* **457** (2016) 3101 [[1601.06120](#)].
- [64] S. Yoshida and Y. Eriguchi, *Rotating boson stars in general relativity*, *Phys. Rev. D* **56** (1997) 762.
- [65] F.E. Schunck and E.W. Mielke, *General relativistic boson stars*, *Class. Quant. Grav.* **20** (2003) R301 [[0801.0307](#)].
- [66] M. Colpi, S.L. Shapiro and I. Wasserman, *Boson Stars: Gravitational Equilibria of Selfinteracting Scalar Fields*, *Phys. Rev. Lett.* **57** (1986) 2485.
- [67] D.J. Kaup, *Klein-Gordon Geon*, *Phys. Rev.* **172** (1968) 1331.
- [68] P.-H. Chavanis, *Mass-radius relation of Newtonian self-gravitating Bose-Einstein condensates with short-range interactions: I. Analytical results*, *Phys. Rev. D* **84** (2011) 043531 [[1103.2050](#)].
- [69] P.-H. Chavanis, *Self-gravitating Bose-Einstein condensates and their connection to dark matter*, *Phys. Rev. D* **106** (2022) 123014 [[2209.03852](#)].
- [70] B. Kleihaus, J. Kunz and S. Schneider, *Stable Phases of Boson Stars*, *Phys. Rev. D* **85** (2012) 024045 [[1109.5858](#)].
- [71] P. Grandclement, C. Somé and E.ourgoulhon, *Models of rotating boson stars and geodesics around them: new type of orbits*, *Phys. Rev. D* **90** (2014) 024068 [[1405.4837](#)].
- [72] M. Vaglio, C. Pacilio, A. Maselli and P. Pani, *Multipolar structure of rotating boson stars*, *Phys. Rev. D* **105** (2022) 124020 [[2203.07442](#)].
- [73] C. Herdeiro, I. Perapechka, E. Radu and Y. Shnir, *Asymptotically flat spinning scalar, Dirac and Proca stars*, *Phys. Lett. B* **797** (2019) 134845 [[1906.05386](#)].
- [74] J.M. Lattimer and M. Prakash, *The physics of neutron stars*, *Science* **304** (2004) 536 [[astro-ph/0405262](#)].
- [75] J.M. Lattimer and M. Prakash, *Neutron star structure and the equation of state*, *Astrophys. J.* **550** (2001) 426 [[astro-ph/0002232](#)].
- [76] H. Heintzmann and E. Hilf, *Neutron star matter and neutron star models*, *Zeitschrift für Naturforschung A* **29** (1974) 269–279.
- [77] B. Carr, A.M. Green and F. Kuhnel, *Primordial Black Holes as a Probe of Cosmology and High Energy Physics*, *Phys. Rept.* **1054** (2024) 1 [[2306.03903](#)].
- [78] A.M. Green and B.J. Kavanagh, *Primordial Black Holes as a dark matter candidate*, *J. Phys. G* **48** (2021) 043001 [[2007.10722](#)].
- [79] S. Hawking, *Gravitationally collapsed objects of very low mass*, *Mon. Not. Roy. Astron. Soc.* **152** (1971) 75.
- [80] B.J. Carr and S.W. Hawking, *Black holes in the early Universe*, *Mon. Not. Roy. Astron. Soc.* **168** (1974) 399.
- [81] B. Carr, F. Kuhnel and L. Sandstad, *Primordial Black Holes as Dark Matter*, *Phys. Rev. D* **94** (2016) 083504 [[1607.06077](#)].
- [82] M. Sasaki, T. Suyama, T. Tanaka and S. Yokoyama, *Primordial Black Hole Scenario for the Gravitational-Wave Event GW150914*, *Phys. Rev. Lett.* **117** (2016) 061101 [[1603.08338](#)].
- [83] Y. Suwa, T. Yoshida, M. Shibata, H. Umeda and K. Takahashi, *On the minimum mass of neutron stars*, *Mon. Not. Roy. Astron. Soc.* **481** (2018) 3305 [[1808.02368](#)].
- [84] K. Kacanja and A.H. Nitz, *A Search for Low-mass Neutron Stars in the Third Observing Run of Advanced LIGO and Virgo*, *Astrophys. J.* **984** (2025) 61 [[2412.05369](#)].

- [85] T. Damour and A. Nagar, *Relativistic tidal properties of neutron stars*, *Phys. Rev. D* **80** (2009) 084035 [[0906.0096](#)].
- [86] E. Poisson, *Tidal deformation of a slowly rotating black hole*, *Phys. Rev. D* **91** (2015) 044004 [[1404.2192](#)].
- [87] J.M. Lattimer, *Neutron Star Mass and Radius Measurements*, *Universe* **5** (2019) 159 [[1912.05750](#)].
- [88] N. Sennett, T. Hinderer, J. Steinhoff, A. Buonanno and S. Ossokine, *Distinguishing Boson Stars from Black Holes and Neutron Stars from Tidal Interactions in Inspiring Binary Systems*, *Phys. Rev. D* **96** (2017) 024002 [[1704.08651](#)].
- [89] T. Chiba and S. Yokoyama, *Spin Distribution of Primordial Black Holes*, *PTEP* **2017** (2017) 083E01 [[1704.06573](#)].
- [90] T. Harada, C.-M. Yoo, K. Kohri and K.-I. Nakao, *Spins of primordial black holes formed in the matter-dominated phase of the Universe*, *Phys. Rev. D* **96** (2017) 083517 [[1707.03595](#)].
- [91] V. De Luca, G. Franciolini, P. Pani and A. Riotto, *The Evolution of Primordial Black Holes and their Spins*, *JCAP* **04** (2020) 052 [[1909.03883](#)].
- [92] M. Evans et al., *A Horizon Study for Cosmic Explorer: Science, Observatories, and Community*, [2109.09882](#).
- [93] M. Punturo et al., *The Einstein Telescope: A third-generation gravitational wave observatory*, *Class. Quant. Grav.* **27** (2010) 194002.
- [94] ET collaboration, *Science Case for the Einstein Telescope*, *JCAP* **03** (2020) 050 [[1912.02622](#)].
- [95] C. García-Quirós, M. Colleoni, S. Husa, H. Estellés, G. Pratten, A. Ramos-Buades et al., *Multimode frequency-domain model for the gravitational wave signal from nonprecessing black-hole binaries*, *Phys. Rev. D* **102** (2020) 064002 [[2001.10914](#)].
- [96] LIGO Scientific Collaboration, Virgo Collaboration and KAGRA Collaboration, “LVK Algorithm Library - LALSuite.” Free software (GPL), 2018. 10.7935/GT1W-FZ16.
- [97] G. Pratten, S. Husa, C. Garcia-Quiros, M. Colleoni, A. Ramos-Buades, H. Estelles et al., *Setting the cornerstone for a family of models for gravitational waves from compact binaries: The dominant harmonic for nonprecessing quasicircular black holes*, *Phys. Rev. D* **102** (2020) 064001 [[2001.11412](#)].
- [98] S. Husa, S. Khan, M. Hannam, M. Pürrer, F. Ohme, X. Jiménez Forteza et al., *Frequency-domain gravitational waves from nonprecessing black-hole binaries. I. New numerical waveforms and anatomy of the signal*, *Phys. Rev. D* **93** (2016) 044006 [[1508.07250](#)].
- [99] S. Khan, S. Husa, M. Hannam, F. Ohme, M. Pürrer, X. Jiménez Forteza et al., *Frequency-domain gravitational waves from nonprecessing black-hole binaries. II. A phenomenological model for the advanced detector era*, *Phys. Rev. D* **93** (2016) 044007 [[1508.07253](#)].
- [100] T. Dietrich, A. Samajdar, S. Khan, N.K. Johnson-McDaniel, R. Dudi and W. Tichy, *Improving the NRTidal model for binary neutron star systems*, *Phys. Rev. D* **100** (2019) 044003 [[1905.06011](#)].
- [101] F. Pannarale, E. Berti, K. Kyutoku, B.D. Lackey and M. Shibata, *Aligned spin neutron star-black hole mergers: a gravitational waveform amplitude model*, *Phys. Rev. D* **92** (2015) 084050 [[1509.00512](#)].
- [102] J.E. Thompson, E. Fauchon-Jones, S. Khan, E. Nitoglia, F. Pannarale, T. Dietrich et al.,

- Modeling the gravitational wave signature of neutron star black hole coalescences*, *Phys. Rev. D* **101** (2020) 124059 [2002.08383].
- [103] Y. Pan, A. Buonanno, J.G. Baker, J. Centrella, B.J. Kelly, S.T. McWilliams et al., *A Data-analysis driven comparison of analytic and numerical coalescing binary waveforms: Nonspinning case*, *Phys. Rev. D* **77** (2008) 024014 [0704.1964].
 - [104] M. Boyle, D.A. Brown and L. Pekowsky, *Comparison of high-accuracy numerical simulations of black-hole binaries with stationary phase post-Newtonian template waveforms for Initial and Advanced LIGO*, *Class. Quant. Grav.* **26** (2009) 114006 [0901.1628].
 - [105] A. Buonanno, B. Iyer, E. Ochsner, Y. Pan and B.S. Sathyaprakash, *Comparison of post-Newtonian templates for compact binary inspiral signals in gravitational-wave detectors*, *Phys. Rev. D* **80** (2009) 084043 [0907.0700].
 - [106] A. Akmal, V.R. Pandharipande and D.G. Ravenhall, *The Equation of state of nucleon matter and neutron star structure*, *Phys. Rev. C* **58** (1998) 1804 [nucl-th/9804027].
 - [107] K. Rink, R. Bachhar, T. Islam, N.E.M. Rifat, K. Gonzalez-Quesada, S.E. Field et al., *Gravitational wave surrogate model for spinning, intermediate mass ratio binaries based on perturbation theory and numerical relativity*, *Phys. Rev. D* **110** (2024) 124069 [2407.18319].
 - [108] B. Gadre, M. Pürrer, S.E. Field, S. Ossokine and V. Varma, *Fully precessing higher-mode surrogate model of effective-one-body waveforms*, *Phys. Rev. D* **110** (2024) 124038 [2203.00381].
 - [109] K.K.H. Lam, K.W.K. Wong and T.D.P. Edwards, *Recalibrating a gravitational wave phenomenological waveform model*, *Phys. Rev. D* **109** (2024) 124009 [2306.17245].
 - [110] F. Ohme, M. Hannam and S. Husa, *Reliability of complete gravitational waveform models for compact binary coalescences*, *Phys. Rev. D* **84** (2011) 064029 [1107.0996].
 - [111] M. Prakash, J.R. Cooke and J.M. Lattimer, *Quark - hadron phase transition in protoneutron stars*, *Phys. Rev. D* **52** (1995) 661.
 - [112] T. Evstafyeva, U. Sperhake, I. Romero-Shaw and M. Agathos, *Gravitational-Wave Data Analysis with High-Precision Numerical Relativity Simulations of Boson Star mergers*, *Physical Review Letters* **133** (2024) 131401.
 - [113] A. Sicilia, A. Lapi, L. Boco, M. Spera, U.N. Di Carlo, M. Mapelli et al., *The Black Hole Mass Function Across Cosmic Times. I. Stellar Black Holes and Light Seed Distribution*, *Astrophys. J.* **924** (2022) 56 [2110.15607].
 - [114] V. Poulin, P.D. Serpico, F. Calore, S. Clesse and K. Kohri, *Cmb bounds on dark matter including pbhs as a candidate*, *Phys. Rev. D* **96** (2017) 083524 [1707.04206].
 - [115] P.D. Serpico, V. Poulin, Y. Inoue and K. Kohri, *Probing pbh dark matter with radio and x-ray observations*, *Phys. Rev. Res.* **2** (2020) 023204 [2002.10771].
 - [116] V. Stasenko, *Redshift evolution of primordial black hole merger rate*, *Phys. Rev. D* **109** (2024) 123546 [2403.11325].
 - [117] R. Ruffini and S. Bonazzola, *Systems of selfgravitating particles in general relativity and the concept of an equation of state*, *Phys. Rev.* **187** (1969) 1767.
 - [118] T. Hinderer, *Tidal Love numbers of neutron stars*, *Astrophys. J.* **677** (2008) 1216 [0711.2420].
 - [119] LIGO SCIENTIFIC, VIRGO collaboration, *GW170817: Measurements of neutron star radii and equation of state*, *Phys. Rev. Lett.* **121** (2018) 161101 [1805.11581].
 - [120] X. Wang, A. Kuerban, J.-J. Geng, F. Xu, X.-L. Zhang, B.-J. Zuo et al., *Tidal deformability of strange quark planets and strange dwarfs*, *Physical Review D* **104** (2021) 123028.